Horn-Shaped Structure Attached to the Ring-Shaped Ion Velocity Distribution during Magnetic Reconnection with a Guide Field*)

Shunsuke USAMI[1,2], Ritoku HORIUCHI[1,3] and Hiroaki OHTANI[1,3]

[1)]*National Institute for Fusion Science, National Institutes of Natural Sciences, Toki 509-5292, Japan*

[2)]*University of Tokyo, Tokyo 113-8654, Japan*

[3)]*Sokendai (The Graduate University of Advanced Studies), Toki 509-5292, Japan*

(Received 9 January 2019 / Accepted 25 June 2019)

The characteristic feature of a "horn-shaped velocity distribution" in magnetic reconnection in the presence of a guide field is investigated by means of simulation and theory. Particle simulations show that a horn-shaped velocity structure is formed in the downstream, concomitant with a ring-shaped velocity distribution studied in the preceding works. The theory which explains the motion of ions responsible for the horn-shaped structure is constructed as an extension of the basic theory for the ring-shaped structure. In the extended theory, ions are accelerated in the inflow direction by an electrostatic field in the separatrix, and thus the gyration speed of such ions in the downstream is larger than that for the basic theory. Test particle simulations confirm that some ions behave as in the extended theory and form the horn-shaped velocity structure.

Keywords: particle simulation, magnetic reconnection, ion heating, PASMO, spherical tokamak

DOI: 10.1585/pfr.14.3401137

1. Introduction

Magnetic reconnection is one of the fundamental processes seen in various plasmas [1], in which magnetic energy is rapidly converted to kinetic and thermal energy of plasma particles. Fusion plasmas are deeply associated with magnetic reconnection processes from both negative and positive aspects. Sawtooth crash or oscillation, which is thought to be related to reconnection, in a tokamak device is a negative aspect. When sawtooth crash or oscillation occurs, the stored energy in the core is released to the periphery region [2]. Hence, the control of sawtooth crash and oscillation is an important issue for fusion plasmas in tokamaks. On the other hand, magnetic reconnection has a positive aspect for merging plasmas in spherical tokamaks, in which plasmas with quite high β are created by plasma heating during magnetic reconnection and are confined [3, 4]. The mechanism of the heating in spherical tokamaks, however, remains unsolved.

We explore the heating mechanism during magnetic reconnection by means of simulation and theory in this work. It is a quite useful and commonly used method to observe and analyze velocity distribution functions for magnetic reconnection studies as shown, for example, in Refs. [5–11]. One can derive where plasma particles are accelerated or heated and what mechanism acts for the plasma acceleration and heating by analyzing velocity distribution. In preceding simulation works by Usami *et al.* [12, 13], on the basis of analyzing ion velocity distribution, an effective heating mechanism during magnetic reconnection in the presence of a guide field was proposed. The essential point of the mechanism is that ions behave as nonadiabatic upon crossing the separatrix, and ring-shaped ion velocity distributions are formed in the downstream of reconnection.

In this paper, an additional anomalous structure, which is observed in the velocity space and is attached to a ring-shaped velocity distribution, is discussed. The organization of this paper is as follows. In Sec. 2, we highlight particle simulation results and review the formation process of a ring-shaped structure of an ion velocity distribution. In Sec. 3, an additional structure, called a "horn-shaped structure," found in particle simulations is shown. We extend the theory for the ring-shaped distribution to explain the formation process of the horn-shaped structure. In addition, we investigate the motion of ions forming the horn-shaped structure by means of test particle simulations. Lastly, section 4 provides a summary of this work.

2. Review of the Ring-Shaped Structure in Velocity Distribution

2.1 Particle simulation method and result

In order to investigate the ion heating mechanism during magnetic reconnection in the presence of a guide magnetic field, we carry out two-dimensional particle simulations, since nongyrotropic motions of plasma electrons and ions, which can not be computed by fluid models, play essential roles in magnetic reconnection, in particular, for

author's e-mail: usami.shunsuke@nifs.ac.jp

*) This article is based on the presentation at the 27th International Toki Conference (ITC27) & the 13th Asia Pacific Plasma Theory Conference (APPTC2018).

plasma heating during magnetic reconnection.

For particle simulations, we use the PASMO code [14,15], in which an open boundary condition is employed. Plasmas are pushed by a driving electric field E_d imposed on the upstream boundary. The driving field E_d supplies particles satisfying a shifted Maxwellian velocity distribution so that plasmas flow into the simulation domain from the upstream boundary. The field E_{dz} is set to zero at the initial time, begins to grow first near the center of the upstream boundary, and eventually has a constant value E_0 in the entire upstream boundary, where E_{dz} is the z-component of E_d. On the other hand, through the downstream boundary, plasma particles can enter and exit freely.

As the initial condition, we take a one-dimensional Harris-type equilibrium with a uniform guide field as Horiuchi and Sato first applied [16]. That is, we set $B_x(y) = B_{x0}\tanh(y/L)$ and $B_z(y) = B_{z0}$ for the magnetic field and $P(y) = P_0 + B_{x0}^2/(8\pi)\mathrm{sech}^2(y/L)$ for the plasma pressure, where B_{x0}, B_{z0}, and P_0 are constants and L is a spatial scale. The temperature is uniform, and the ion temperature is taken to be equal to the electron temperature: $T_{i0}/T_{e0} = 1.0$.

The simulation parameters are denoted as follows. The simulation domain size is $10.54(c/\omega_{pi}) \times 2.63(c/\omega_{pi})$, where c is the speed of light and ω_{pi} is the ion plasma frequency. The initial numbers of electrons and of ions are 14,090,240, respectively. The ion-to-electron mass ratio is taken to be $m_i/m_e = 100$. The ratio of the electron plasma frequency to the electron gyrofrequency is $\omega_{pe}/\omega_{ce} = 6.0$, where $\omega_{ce} = eB_{x0}/(m_e c)$ is defined. Thus, the Alfvén speed is expressed as $v_A/c = 0.037$ for the total magnetic field $B_0 = \sqrt{B_{x0}^2 + B_{z0}^2}$. The time step is $\omega_{pi}\Delta t = 0.0052$, and the grid spacing is $\Delta_g/(c/\omega_{pi}) = 0.010$.

We demonstrate results of a simulation run under the following parameter values: $B_{z0}/B_{x0} = 2$, $L/(c/\omega_{pi}) = 0.66$, $P_0/(B_{x0}^2/8\pi) = 0.35$, and $E_0/B_{x0} = -0.04$. This simulation run is the same as a run which has been performed in Refs. [12, 13]. Figure 1 (a) shows the spatial profile of the ion temperature perpendicular to the local magnetic field as color contours and the magnetic field lines at $\omega_{pi}t = 775$. Magnetic reconnection is driven by inflow plasmas supplied from the upstream boundary, and the reconnection point (the X-point) is located at the center of the simulation domain $(x, y) \simeq (0, 0)$. An ambipolar reconnection outflow emanates from the X-point. We can clearly see that the ion temperature rises mainly in the downstream. Figures 2 (a) - (d) display ion velocity distributions at the local areas (A) - (D) represented in Fig. 1, respectively. As Refs. [12] and [13] demonstrated, ring-shaped velocity distributions are formed, which means that the velocity distributions are expanded and ions are effectively heated in the downstream.

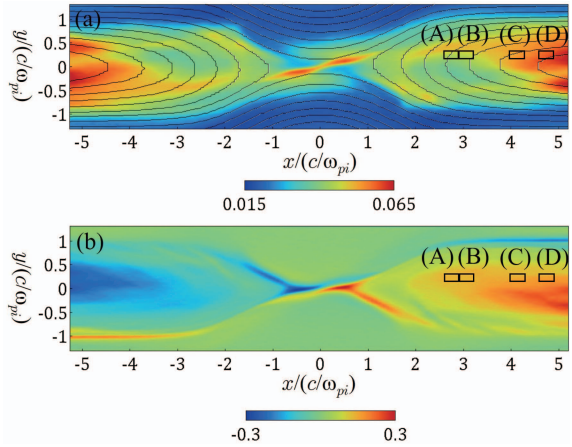

Fig. 1 (a) Spatial profiles of the ion temperature perpendicular to the local magnetic field as the color contours and the magnetic field lines. (b) Spatial profile of the electric field E_y. The local areas (A) - (D) indicated in the panels (a) and (b) are in the downstream, primarily where the ion temperature is increased. In the lower-side separatrix for $x > 0$ and in the upper-side separatrix for $x < 0$, a strong E_y exists.

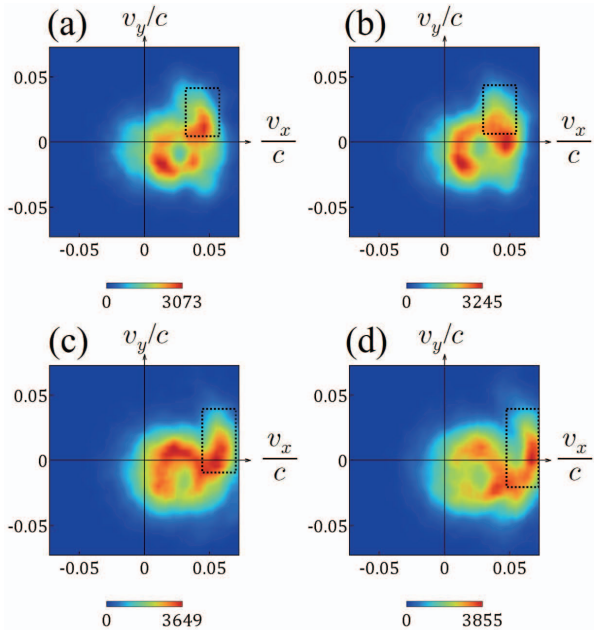

Fig. 2 Ion velocity distributions in the local areas (A) - (D) of Fig. 1. The regions surrounded by the dotted lines denote horn-shaped structures. In all the panels (a) - (d), ring-shaped and horn-shaped structures are shown.

2.2 Basic theory

The formation process of the ring-shaped velocity distribution has been elucidated as the following basic theory [12]. A large percentage of ions move from the upstream across the separatrix into the downstream, and these ions are responsible for the formation of the ring-shaped distribution. The separatrix width is quite thin for ions. Hence, ions behave as nonadiabatic upon crossing the separatrix [7, 12, 13]. In the basic theory, when ions enter the downstream across the separatrix, their entry speed is suf-

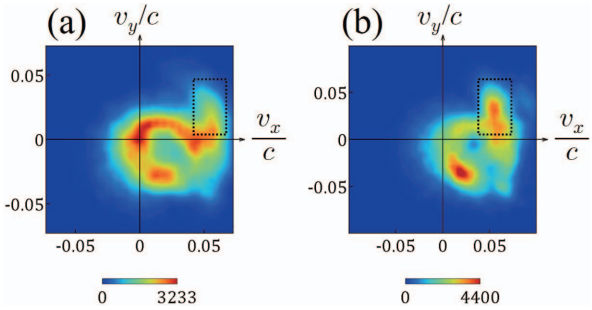

Fig. 3 Ion velocity distributions (a) at an earlier phase for the same run of simulations as in Fig. 2, and (b) for a different run of simulations under a different value of the driving electric field. The regions surrounded by the dotted lines denote horn-shaped structures. Horn-shaped and ring-shaped structures are seen in both panels.

ficiently small so that we regard it as zero for the ideal case. Here it is assumed for simplification that in the downstream, the reconnection outflow is in the x direction and its speed is $u_{\rm out}$, and the guide magnetic field in the z direction and the convective electric field in the y direction are uniform. The other components of the electromagnetic field can be ignored because they are much smaller. The ions move in the x direction owing to the $E \times B$ drift while in gyromotion around the guide magnetic field in the downstream. It is characteristic that the drift speed is equal to $u_{\rm out}$, and the gyration speed is also equal to $u_{\rm out}$. The ring-shaped velocity distribution consists of such ions. The effective temperature of the ions forming the ring-shaped distribution is simply given as $T_i = 1/2\, m_i u_{\rm out}^2$.

3. Horn-Shaped Structure in Velocity Distribution

3.1 Particle simulation result

In the velocity distribution of Fig. 2, we can observe another characteristic structure surrounded by dotted lines, in addition to the ring-shaped structure. We call this a "horn-shaped structure or distribution." Such horn-shaped structures are seen not only for this run of simulations, but also for various runs of simulations. We further show ion velocity distributions in Fig. 3. The panel (a) is an ion velocity distribution at an earlier phase ($\omega_{pi}t = 258$) for the same run of the simulations as in Fig. 2, and the panel (b) is an ion velocity distribution for a different run of simulations with a different value of the driving electric field $E_0/B_{x0} = -0.06$. Horn-shaped structures can be seen in both cases.

3.2 Extended theory

We extend the basic theory in order to explain the formation mechanism of a horn-shaped structure. If some ions are accelerated in the y direction by an electrostatic field E_y in the separatrix, they have a finite speed v_y when they enter the downstream [8, 17, 18]. Actually, Fig. 1 (b) shows that E_y is strong in the lower-side separatrix for $x > 0$ and in the upper-side separatrix for $x < 0$. In some observational studies in the geomagnetosphere, it has been reported that ions are accelerated by an electric field in the separatrix [19, 20].

Let the entry velocity of the ions be $(0, v_{y0})$, where it is noted that the value of v_{y0} can be different for each ion. For the electromagnetic field in the downstream, we employ the same assumption as the basic theory. In the downstream, the motion of the ions is the $E \times B$ drift while in gyromotion as described in the basic theory. The gyration speed, however, is different from the gyration speed in the basic theory. The gyration speed is given as $\sqrt{u_{\rm out}^2 + v_{y0}^2}$, which is larger than $u_{\rm out}$. In the velocity space, the ions are located outside a circle whose radius is $u_{\rm out}$ (a ring-shaped structure). Under the above situation, let us observe a velocity distribution in a local area. Assuming that gyromotion phases of the ions are limited within a narrow range, the velocity distribution formed by the ions is not a ring-shape, but a horn-shape.

In the extended theory, it is essential that ions are not sufficiently accelerated in the x direction in the separatrix. If an ion is accelerated in the x and y directions in the separatrix, it has a finite entry velocity (v_{x0}, v_{y0}). The gyration speed is expressed as $\sqrt{(u_{\rm out} - v_{x0})^2 + v_{y0}^2}$. The large v_{x0} makes the gyration speed of the ion decrease. Consequently, a horn-shaped structure would not be seen, because a structure formed by such ions whose gyration speed is smaller would overlap the ring-shaped distribution.

3.3 Test particle simulation

In order to show that a horn-shaped structure is formed by ions expressed by the extended theory, we perform test particle simulations. The method for test particle simulations is as follows. Before test particle simulations, we perform a particle simulation by using the PASMO code and obtain the electromagnetic field data under a steady state of magnetic reconnection. The equations of motion for test ion particles are calculated in the given electromagnetic field.

We trace the motions of 60,000 test ion particles, and demonstrate the positions of the ion particles at various times (a) $\omega_{pi}\tau = 0$, (b) 60, (c) 120, and (d) 240 in Fig. 4. For distinguishing the time in the test particle simulation from the time in the particle simulations by the PASMO code, we use τ as the time in the test particle simulation. The panel (a) shows that the initial positions of the test ions are set on the upper-side upstream boundary $y/(c/\omega_{pi}) = 1.31$ and on the lower-side upstream boundary $y/(c/\omega_{pi}) = -1.31$. The x-coordinate of the initial position is uniformly distributed within $-4.0 < x/(c/\omega_{pi}) < 4.0$. The number of the test ions which initially are set on each side of the upstream boundary is 30,000. The black and blue points correspond to the test ions whose initial posi-

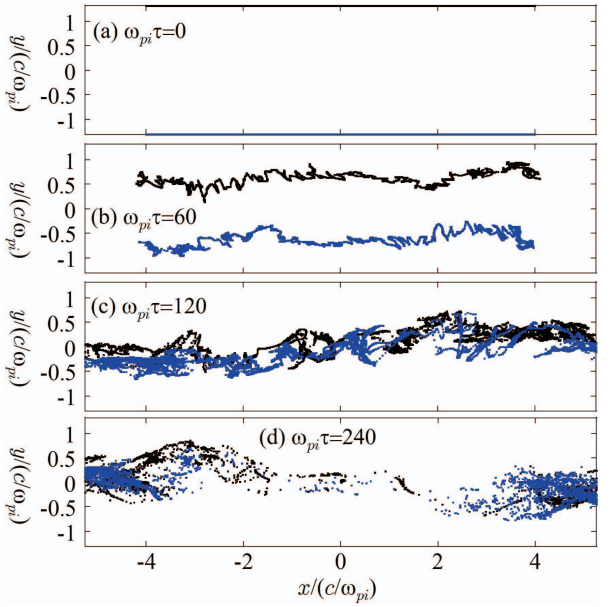

Fig. 4 Positions of the ion particles calculated by a test particle simulation at various times. The black and blue points denote the ions coming from the upper-side and lower-side upstream boundaries, respectively.

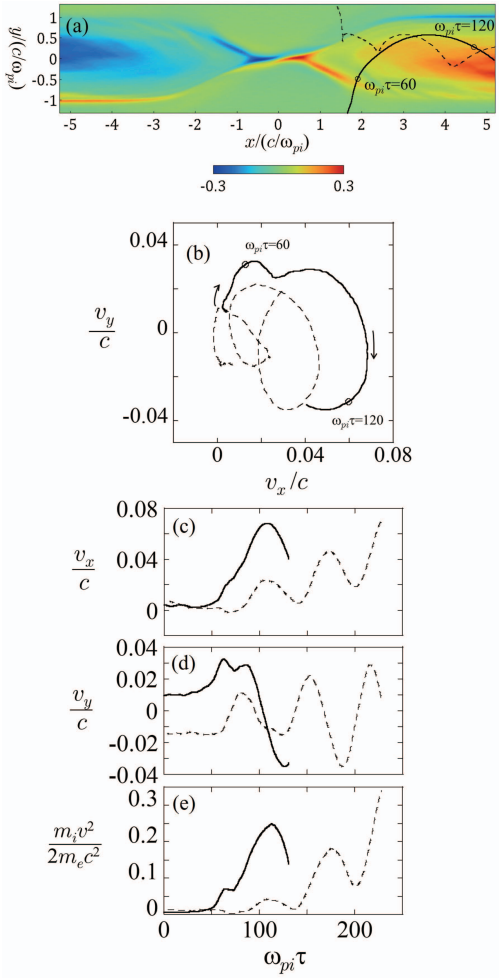

Fig. 5 Motion of an ion particle calculated by a test particle simulation. The panels (a), (b), (c), (d), and (e) plot the orbit in the (x, y) plane, the orbit in the (v_x, v_y) plane, the time evolution of v_x, v_y, and the kinetic energy, respectively. The solid and dashed lines denote ions based on the basic and extended theories, respectively. The color contours in the panel (a) indicate the electric field E_y.

tions are on the upper- and lower-side upstream boundary, respectively. Each test ion has an initial velocity equal to the ion fluid velocity, which has been obtained by the particle simulation, at each local position. At $\omega_{pi}\tau = 60$ (the panel (b)), the ions from the upper-side upstream move in the $-y$ direction, and the ions from the lower-side upstream move in the y direction. At $\omega_{pi}\tau = 120$ (the panel (c)), the black and blue points mix. Hence, we can find that the ions coming from both sides converge and co-exist in the same region. At $\omega_{pi}\tau = 240$ (the panel (d)), which is the termination time of the test particle simulation, a large part of ions already escaped from the simulation domain across the downstream boundary.

We would like to explain that the formation of a horn-shaped structure is responsible for ions coming from the lower-side upstream. We plot the orbit, velocity, and kinetic energy of a typical ion particle in Fig. 5. Here, we call an ion particle described by the extended theory "EX-ion," while we call an ion expressed within the basic theory "BS-ion." The solid lines denote a typical EX-ion, and the dashed lines represent a BS-ion, which was introduced in Ref. [13], for comparison.

Figure 5 (a) shows the orbits of the ion particles, where the color contours indicate the electric field E_y. Let us concentrate on the half region $x > 0$. We find that the lower-side separatrix is wider than the upper-side separatrix, and a large E_y exists in the lower-side separatrix. The EX-ion is accelerated in the y direction across the lower-side separatrix. In the downstream, the EX-ion moves in the x direction with oscillating owing to the $E \times B$ drift and the gyromotion. The amplitude of the gyration is larger than that for the BS-ion.

Figure 5 (b) shows the ion orbits in the velocity space (v_x, v_y). When the EX-ion enters the downstream at $\omega_{pi}\tau \simeq 60$, the EX-ion has a large v_y. Hence, the velocity circle of the EX-ion is larger than that of the BS-ion.

Further, we plot the time development of velocity components v_x and v_y in Figs. 5 (c) and (d). At $\omega_{pi}\tau \simeq 60$, when the EX-ion enters the downstream, the EX-ion has a small v_x and a large v_y, which is consistent with the extended theory. After that, v_x is increased and v_y is decreased because of the transformation from v_y to v_x owing to the gyromotion. In contrast, at $\omega_{pi}\tau \simeq 140$, when the BS-ion is in the downstream (This is the re-entry. See Ref. [13] for details.), v_x and v_y of the BS-ion are small, which is consistent with the basic theory.

Lastly, we plot the time evolution of the kinetic energy in Fig. 5 (e). At $\omega_{pi}\tau \simeq 60$ (the entry time of the EX-ion), the EX-ion has large kinetic energy. In the downstream, the

EX-ion further gains kinetic energy from the convective electric field, the main component of which is E_y. Compared with the BS-ion at the same time τ, the EX-ion has much larger kinetic energy. We can explain the larger increase in the kinetic energy of the EX-ion as follows. In both the basic and the extended theories, the electromagnetic field is assumed to be uniform. However, in particular E_y becomes larger in a deeper downstream (x is larger). The EX-ion moves to the deeper downstream (stronger E_y region) earlier than the BS-ion. Hence, at the same time τ, the kinetic energy of the EX-ion is much larger than that of the BS-ion.

We discuss not only the behavior of a single particle, but also motions of many particles. In the following figures, we display not only the particles which are in a local area at the instance $\omega_{pi}\tau = 240$, but the particles which were and are in a local area by $\omega_{pi}\tau = 240$. In other words, we record the particle data every $\omega_{pi}\delta\tau = 3$, and treat an identical particle at a past time as a different particle. Thus, it is noted that some particles are displayed in the following figures multiple times. The reason is as follows. We set all the ion particles on the upstream boundary at $\omega_{pi}\tau = 0$. We do not supply new particles after the initial time. Under a steady state of reconnection, however, particles should continuously flow inward from the upstream with a constant flux. Instead of continuous supply of particles from the upstream, we accumulate the temporal sequence data of the particles during $\omega_{pi}\tau = 0$ - 240 in order to mimic continuous inflow plasmas under a steady state.

In Fig. 6, we plot velocities (v_x, v_y) of the particles inside the local area whose location is the same as the area (A) of Fig. 1. The panels (a) and (b) show the ions from the upper-side upstream and from the lower-side upstream, respectively. A ring-shaped structure is clearly seen in the panel (a) and a horn-shaped structure is found in the panel (b). We can understand that the ions from the upper-side upstream dominantly form the ring-shaped structure and the ions from the lower-side upstream form the horn-shaped structure. The panel (c), which is a superimposed figure of the panels (a) and (b), reproduces the entire structure seen in Fig. 2 (a).

Here, it is noted that horn-shaped structure has a finite width in the direction of the ring center and hence the horn is attached to the ring. The ion velocity distributions obtained in our particle simulations also indicate that the horns are attached to the rings. A reason for the attachment of the rings and the horns can be explained as follows. An electrostatic field in the separatrix is not uniform [11]. Ions from the lower-side upstream pass through slightly different positions in the lower-side separatrix and are accelerated to slightly different entry velocities. Thus, the horn-shaped structure has a finite width in the direction of the ring center and thus is attached to the ring-shaped structure. Discussed in more detail, the acceleration in the x direction by E_x, which decreases the gyration speed, i.e., the velocity radius in the velocity space as described in

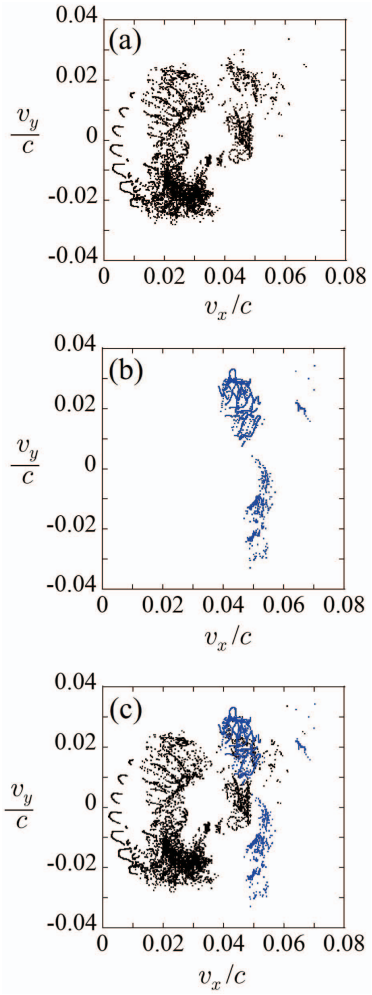

Fig. 6 Positions of the ions inside the local area (A) in Fig. 1 calculated by a test particle simulation. The panel (a) shows that the ions from the upper-side upstream form the ring-shaped structure, and the panel (b) displays that the ions from the lower-side upstream form the horn-shaped structure. The panel (c) is a superimposed figure of the panels (a) and (b).

Sec. 3.2, plays a partial role in a finite width of the horn-shaped structure. The same holds true for the basic theory. A finite width of the ring also contributes to the attachment between the ring and the horn. In the idealized case of the basic theory, the ion entry speed is regarded as zero. However, the entry velocities of ions are small, but not completely zero. The ions have slightly different entry velocities, because a non-uniform electrostatic field, which is weaker than in the lower-side separatrix, exists in the upper-side separatrix. This makes the width of ring-shaped structures be finite.

Let us discuss why the ions from the lower-side upstream do not form a ring-shaped structure, but construct a horn-shaped structure in the local area (A). In other words, we discuss how the gyromotion phases of the ions from the lower-side upstream are limited within a narrow range. In Fig. 7, we depict the number of particles vs x_0, the initial

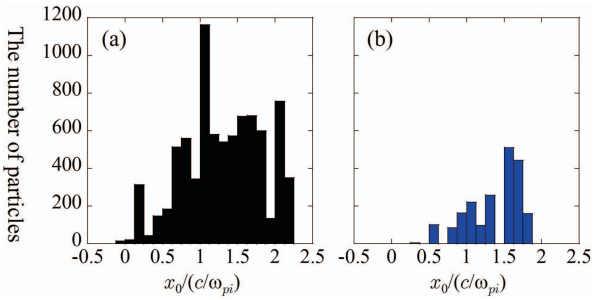

Fig. 7 The number of ion particles vs the initial positions (a) for the ions from the upper-upstream and (b) for the ions from the lower-upstream, inside the local area (A) of Fig. 1.

x-positions of ions which are inside the local area, (a) for the particles from the upper-side upstream and (b) for the particles from the lower-side upstream. Among the total number of ions, the ratio of the ions from the upper-side upstream and from the lower-side upstream are approximately 80% and 20%. Ions whose initial positions are within a wide range of $-0.013 < x_0/(c/\omega_{pi}) < 2.17$ (a standard deviation of 0.52) from the upper-side upstream can enter the local area (A), while ions whose initial positions are within a narrow range of $0.190 < x_0/(c/\omega_{pi}) < 1.79$ (a standard deviation of 0.34) from the lower-side upstream can enter the local area (A). This result would be one of the important factors leading to bias of gyromotion phases of the ions from the lower-side upstream inside the local area. In other words, it would be inevitable that upon entering the downstream across the lower-side separatrix, almost ions obtain gyromotion phases which will occupy the dotted-line box in Fig. 2 (a) when they later arrive at the position of the boxed area (A).

4. Summary

By means of particle and test particle simulations and theory, we have studied a horn-shaped structure of ions in the velocity space in magnetic reconnection with a guide magnetic field. In particle simulations, the horn-shaped structure has been found as an additional structure to a ring-shaped velocity distribution. In our previous works, we have constructed the basic theory explaining the formation process of the ring-shaped structure. In this work, we have improved the basic theory to construct the extended theory for the formation mechanism of the horn-shaped structure. In the basic theory, ions enter the downstream across the separatrix with zero velocity. In the extended theory, ions are accelerated perpendicular to the outflow direction (in the inflow direction) upon crossing the separatrix, and thus enter the downstream with a finite velocity perpendicular to the outflow. The gyration speed of the ions is larger than that for the basic theory. By means of test particle simulations, it has been confirmed that the motion of ions coming from the lower-side upstream is based on the extended theory, because a strong electrostatic field exists in the lower-side separatrix (for the $x > 0$ region). Furthermore, test particle simulations have demonstrated that the ions responsible for the extended theory inside a local area have gyromotion phases limited within a narrow range, and consequently the horn-shaped structure is formed in the velocity space.

In this work, we have focused on the formation process of anomalous velocity distributions in the downstream region close to the X-point (within $\sim 5c/\omega_{pi}$). A larger-scale simulation, for instance, Ref. [21] indicates that the ion acceleration mechanism is changed in the far downstream region. In such a far downstream, ion velocity distributions will be changed from the ring-shaped and horn-shaped structures.

Acknowledgments

This simulation work was performed on "Plasma Simulator" (FUJITSU FX100) at the National Institute for Fusion Science. This work was partially supported by a Grant-in-Aid for Scientific Research from the Japan Society for the Promotion of Science (KAKENHI 16K17847), the Research Cooperation Program on "Hierarchy and Holism in Natural Sciences" and "Magnetic Reconnection Studies with Kinetic Simulations" at the National Institutes of Natural Sciences, the General Coordinated Research at the National Institute for Fusion Science (NIFS17KNWS003, NIFS18KNTS055, NIFS17KNSS100), and "Joint Usage/Research Center for Interdisciplinary Large-scale Information Infrastructures" and "High Performance Computing Infrastructure" in Japan.

[1] M. Yamada, R. Kulsrud and H. Ji, Rev. Mod. Phys. **82**, 603 (2010).
[2] H.K. Park, N.C. Lühmann Jr., J.H. Donn, I.G.J. Glassen, C.W. Domie, E. Mazzucato, T. Munsat, N.J. van de Pol, Z. Xia and TEXTOR team, Phys. Rev. Lett. **96**, 195003 (2006).
[3] Y. Ono, Y. Hayashi, T. Ii, H. Tanabe, S. Ito, A. Kuwahata, T. Ito, Y. Kamino, T. Yamada, M. Inomoto and TS-Group, Phys. Plasmas **18**, 112113 (2011).
[4] Y. Ono, H. Tanabe, T. Yamada, M. Inomoto, T. Ii, S. Inoue, K. Gi, T. Watanabe, M. Gryaznevich, R. Scannell, C. Michael and C.Z. Cheng, Plasma Phys. Control. Fusion **54**, 124039 (2012).
[5] M. Hoshino, T. Mukai, T. Yamamoto and S. Kokubun, J. Geophys. Res. **103**, 4509 (1998).
[6] M. Hesse, M. Kuznetsova and J. Birn, Phys. Plasmas **11**, 5387 (2004).
[7] J.F. Drake, P.A. Cassak, M.A. Shay, M. Swisdak and E. Quataert, Astrophys. J. **700**, L16 (2009).
[8] C.Z. Cheng, S. Inoue, Y. Ono and R. Horiuchi, Phys. Plasmas **22**, 101205 (2015).
[9] S. Zenitani, H. Hasegawa and T. Nagai, J. Geophys. Res. Space Physics **122**, 7396 (2017).
[10] F. Pucci, S. Usami, H. Ji, X. Guo, R. Horiuchi, S. Okamura, W. Fox, J. Jara-Almonte, M. Yamada and J. Yoo, Phys.

Plasmas **25**, 122111 (2018).
[11] M. Hesse, C. Norgren, P. Tenfjord, J.L. Burch, Y.-H, Liu, L.-J. Chen, N. Bessho, S. Wang, R. Nakamura, J.P. Eastwood, M. Hoshino, R.B. Torbert and R.E. Ergun, Phys. Plasmas **25**, 122902 (2018).
[12] S. Usami, R. Horiuchi and H. Ohtani, Phys. Plasmas **24**, 092101 (2017).
[13] S. Usami, R. Horiuchi, H. Ohtani, Y. Ono and H. Tanabe, Plasma Fusion Res. **13**, 3401025 (2018).
[14] W. Pei, R. Horiuchi and T. Sato, Phys. Rev. Lett. **87**, 235003 (2001).
[15] H. Ohtani and R. Horiuchi, Plasma Fusion Res. **4**, 024 (2009).
[16] R. Horiuchi and T. Sato, Phys. Plasmas **4**, 277 (1997).
[17] N. Aunai, G. Belmont and R. Smets, J. Geophys. Res. **116**, A09232 (2011).
[18] R. Horiuchi, S. Usami and H. Ohtani, Plasma Fusion Res. **9**, 1401092 (2014).
[19] J.R. Wygant, C.A. Cattell, R. Lysak, Y. Song, J. Dombeck, J. McFadden, F.S. Mozer, C.W. Carlson, G. Parks, E.A. Lucek, A. Balogh, M. Andre, H. Reme, M. Hesse and C. Mouikis, J. Geophys. Res. **110**, A09206 (2005).
[20] L.-J. Chen, N. Bessho, B. Lefebvre, H. Vaith, A. Fazakerley, A. Bhattacharjee, P.A. Puhl-Quinn, A. Runov, Y. Khotyaintsev, A. Vaivads, E. Georgescu and R. Torbert, J. Geophys. Res. **6**, A12213 (2008).
[21] K. Fujimoto, Front. Phys. **6**, 119 (2018).